Computational Polymer Dynamics via DL_POLY

DB Adolf*†, SN Butler†, PM Drew†, S Hotston†, K, Karatasos‡

†University of Leeds
School of Physics and Astronomy
Leeds LS2 9JT

‡University of Thessaloniki
Department of Chemical Engineering
Section of Chemistry
Physical Chemistry Lab
PO Box 420
54124 Thessaloniki Greece

A review is presented of recent work in the group utilising the DL_POLY molecular dynamics package. Simulations have been performed across several areas of polymer physics including the dynamics of polyethylene as a function of density and chain length, the rheology of trifunctional dendrimers, and penetrant diffusion with a macromolecular matrix. The methodology and conclusions of these investigations are reviewed.

Keywords: DL_POLY; polymers; simulation; dynamics

Introduction

With the explosion in affordable computational power, ready access to sophisticated molecular modelling software grows accordingly. The forms of these packages vary from suites of commercial applications to standalone programmes. Applications on the commercial end often come with in-built forcefield data while others allow the user to code in parameters directly. Standalone programmes offer the user the ability to modify the source code directly for some

* Corresponding Author: d.b.adolf@leeds.ac.uk + 44 (0)113 3433812

targeted project whereas others offer some flexibility through scripting languages. DL_POLY [1] is one such package and offers many attractive features. This paper summarises three distinct polymer modelling projects which have employed DL_POLY within the group.

Section A - Density and Pressure Effects on Polymer Dynamics.

Global polymer dynamics within bulk, unentangled systems are known to be described well by the Rouse model or one of its variants. However, as one considers fast segmental motions on shorter length scales, the Rouse model fails since the Gaussian assumption associated with it no longer holds. This failure is attributed to the details of local structure becoming increasingly more important when describing polymer dynamics on progressively shorter lengthscales. At the same time, aspects of longer length relaxations are known to influence these segmental motions [2] and the symbiosis between short and long length scale polymer dynamics is at the heart of polymer structure-property relationships. Segmental dynamics are closely linked with polymer structure while the role of longer length motions in polymer properties is well established. To further calibrate the understanding of polymer motion, Karatasos and Adolf employed DL_POLY in a study of the short and long length scale polymer dynamics of united atom non-entangled linear polyethylene as a function of density. The simulated systems were comprised of either 50 chains of 20 united atoms (i.e 50/20 system) or 10 chains of 100 united atoms (i.e. 10/100 system). Simulations were equilibrated within the NVT ensemble at 400K for 4 nanoseconds followed by 18 nanoseconds of production within the NVE ensemble. Further details concerning equilibration, production and parameterisation are found in previous publications [3][4].

Chain reorientational dynamics were analysed in terms of autocorrelation functions (ACFs) of second order Legendre polynomials (P_2) involving unit vectors in the direction of various

chords, $\mathbf{c}_k$, connecting k successive bonds along the backbone. A model independent approach was adopted in quantitatively comparing the decay of the various ACFs by assuming a continuous distribution of exponential processes through the use of the expression

$$C(t) = \int_0^\infty F[\ln(\tau)]\exp[-\frac{t}{\tau}]d\ln\tau \qquad (1)$$

where $F[\ln(\tau)]$ denotes the normalised distribution of relaxation times (DRTs) [5][6]. Distinct relaxation processes are easily identified through the DRT peaks while the peak widths give insight into the dispersion of the exponential decays. Figures 1 and 2 summarise the findings of this study with the former corresponding to the 50/20 system and the latter to the 10/100 system.

< figures 1 & 2 side by side here >

For the 50/20 system, the DRTs for chords ranging from bonds (i.e. k=1) to the end-to-end vector each exhibit a single peaking implying a single dynamical process. As the density increases, the DRTs begin to exhibit two peaks. Generally speaking, one process tends to be on the timescale of the bond vector while the second hovers around the timescale of the end-to-end vector. Figure 2 reveals similar DRT plots for the 10/100 system. At the lowest density, a single peak with a broadening tail is observed while a two peaked DRT is seen for the end-to-end vector. DRTs for various k values at the intermediate density are qualitatively similar to their low density cousins at low values of k. As k increases, the DRTs become increasingly broader until the DRT for the end-to-end vector is reached where a crisp three peaked structure is clearly seen. This three peaked structure is observed in most DRTs at the highest density. The absence of the intermediate peak within the 50/20 system suggests the intermediate peak corresponds to a response in the chain dynamics to the combined effect of density and chain length. This behavior is in the spirit of earlier studies suggesting the chain axis relaxation of a given chain is restricted by a pipe whose

boundaries are defined by neighbouring chains [7]. Furthermore, the behaviour of the DRTS is consistent with NMR experiments of melt polyethylene where the backbone is comprised of 153 carbon atoms [8]. Analysis revealed a motional process on the timescale between fast local dynamics and significantly slow global dynamics is required.

A corresponding DL_POLY study into the effect of pressure on the dynamics of polyethylene was also performed. High pressures are confronted in polymer processing and applications though studies addressing the influence of such pressures on polymer dynamics are scarce especially in comparison to studies focusing on the influence of temperature on polymer dynamics. The previous 50/20 and 10/100 systems discussed previously were simulated in the NpT ensemble employing several forcefields [9-12] at temperatures between 375K and 475K each at pressures of 1 bar, 1 kbar and 5 kbar. Some of these forcefields required DL_POLY to be modified to accept the functional form of some of the associated potentials. A broad area of analysis was covered encompassing transition rates, static and dynamic torsional angle coupling, and geometric autocorrelation functions. The results of these investigations can be found in a previous publication[13]. The intermediate DRT peak discussed in the previous study was also observed within this study. In particular, high pressure melts exhibited this peak at shorter $\mathbf{c}_k$ vectors (i.e. smaller numerical values of k) relative to similar runs at ambient pressure.

Section B - Rheology of Dendrimers.

This study employed DL_POLY to investigate the intrinsic viscosity behaviour of trifunctional dendrimers. These are highly branched molecules which possess a focal core surrounded by concentric layers or generations of monomers. Interest in these materials grew when their intrinsic viscosity was shown to peak as molecular weight increased. This is in contrast with linear polymer

chains where intrinsic viscosity increases steadily with molecular weight according to the Mark Houwink relationship. This behaviour earmarked dendrimers as potential viscosity modifiers. Previous to the study to be discussed here, a large portion of the computational work involving dendrimers adopted a stochastic approach in which the solvent is represented as a structureless continuum. Such efforts did reveal a peak in the computational intrinsic viscosity at similar generations where the peak is seen experimentally. However, the appearance of the peak was seen by some studies to be dependent on whether additional hydrodynamic interactions were directly input into the simulations via expressions like the Rotne-Prager-Yamakawa interaction tensor.

Our efforts in the current study under discussion were aimed at investigating how computational dendrimer intrinsic viscosity behaviour generated from explicit solvent NVT equilibrium molecular dynamics (EQMD) simulations coupled with Green-Kubo relationships compared to previous stochastic approaches. Complete simulation details of this study are found in a recent publication [14]. In general, these efforts were divided into two paths both using a system of 4122 particles in total (i.e. dendrimer + solvent). One path employs the Green-Kubo expression for shear viscosity, η, depicted in equation (2) as the integral of the $\alpha\beta^{th}$ component of the stress autocorrelation function.

$$\eta = \frac{V}{k_B T}\int_0^{\infty} \left\langle P_{\alpha\beta}(0) P_{\alpha\beta}(t) \right\rangle dt \qquad (2)$$

T is the temperature of the system, and the angle brackets denote an average over all time origins. For a system of N particles (i.e. dendrimer + solvent) $P_{\alpha\beta}$ as is written as

$$P_{\alpha\beta} = \frac{1}{V}\left[\sum_{i=1}^{N} m_i \underline{v}_{i,\alpha}\underline{v}_{i,\beta} + \sum_{i=1}^{N}\sum_{j>i}^{N} \underline{F}_{ij,\alpha}\underline{r}_{ij,\beta}\right] \qquad (3).$$

It has the units of pressure and represents a generalised component of the complete stress tensor, $\underline{\mathbf{P}}$. The right hand side of equation (3) is composed of two terms with the first representing kinetic

energy and the second denoting contributions from the virial. V in equation (3) represents the simulation volume. An estimate from the intrinsic viscosity of a solution state dendrimer system is then generated using equation (4)

$$IV = \lim_{c \to 0} \frac{\eta - \eta_s}{\eta_s c}. \qquad (4)$$

where η and η_s are the solution and solvent viscosities respectively with c being the concentration of solvent in units of g ml^{-1}.

The second path followed in this study originates from the fact that η and η_s in equation (4) often differ slightly in a quantitative sense as intrinsic viscosity is a measure of how a solute (i.e. dendrimer) changes the viscosity of the solvent. The resulting numerator is often small in value and susceptible to large error bars. A means around this complication is afforded by Stockmayer *et al* [15] who presented an alternative Green-Kubo expression that allows the numerator in equation (4) to be calculated directly from a solution simulation. The expression can be generated by considering the identities of the particles within the summations of the stress tensor. The organised and transparent manner in which DL_POLY is written allowed the construction of the stress tensor components to be split into three parts. One part, P_u, segregates the contributions from the solute while another part, P_s, considers only contributions from the solvent. The remaining part, P_m, considers solvent-solute mixed contributions. Replacing $P_{\alpha\beta}$ in equation (2) with this sum of three terms yields three autocorrelation functions in addition to six cross correlation functions. Assuming all auto and cross correlations involving P_m in addition to cross correlations between P_u and P_s are negligible, the two surviving autocorrelations of P_u and P_s offer a direct route to the numerator in equation (4) as follows

$$\eta_{diff} = \eta - \eta_s = \frac{V}{k_B T} \int_0^\infty \langle P_u(0) P_u(t) \rangle dt \qquad (5)$$

to yield an alternative route to IV data as

$$IV = \lim_{c \to 0} \frac{\eta_{diff}}{\eta_s c}. \qquad (6)$$

It is important to emphasise that this approach directly generates the numerator of the equation (4) as opposed to the first path where the numerator is generated via a difference of two comparable terms. Furthermore, the hunt for the intrinsic viscosity peak is performed for a series of dendrimers in the same LJ solvent rendering it a relative comparison and hence dispensing with the need for any η_s simulation data.

< figure 3 here >

Figure 3 reveals simulated data using equation (4) and equation (6) in addition to Brownian dynamics (BD) results from Lyulin et al [16]. The observed agreement between the two EQMD approaches and their joint agreement with the BD data is excellent. In all cases, a maximum in the intrinsic viscosity is found at generation 5. The agreement between data generated from the two different Green Kubo expressions reveal the assumptions used to generate equation (6) are valid.

Section C- Gas Diffusion through Poly(ethylene terephthalate).

Recent efforts in the group have focused on modelling gas diffusion processes through polyethylene terephthalate (PET). Recent experimental work has revealed that the solubility of nitrogen in PET is dramatically affected by the additional presence of oxygen and carbon dioxide [17]. The former served to reduce the solubility of nitrogen, perhaps by competing for occupation sites with nitrogen or by reducing the favourability of nitrogen occupation at those sites. In contrast, carbon dioxide appears to swell the polymer structure providing a greater free volume for diffusion. Crucially, the opposite effect of oxygen and carbon dioxide appears to suggest that the effect does not have a solely steric origin. Accurate simulation of the dynamics of small penetrants has historically

proven to be challenging. Initial efforts consisted of treating the motion of the penetrants as a series of thermally activated jumps between cavities defined the structure of the surrounding polymer matrix. These cavities essentially behaved as three-dimensional potential wells with the rate at which the penetrants moved between them calculated via a transition state theory (TST) approach. The computationally intensive problem of simulating both the solute and the surrounding polymer was simplified by considering two progressive approximations. The first suggests that the motion of small molecules through a bulk amorphous polymer is dependent only on the elastic motion of the polymer [18]. The second considers the polymer matrix as a rigid obstacle to the motion of small penetrants on the timescale of the motion of those penetrants [19]. These approaches have been useful in accurately simulating the spatial trajectories of small penetrants and, as a result, their concentration profile. However, the recent and continuing rapid increase in computational power available to researchers allows penetrant motion studies to be performed systematically (i.e. as a function of several key variables of interest) using conventional molecular dynamics techniques to generate a collection of trajectories tens of nanoseconds in length using relevant polymer systems such as PET. Kikuchi and co-workers recently attempted to pursue such an approach using a binary gas/polymer phase to the calculation of the transport co-efficients of gases in polyisoprene and reported that, under such conditions, NpT simulations suffer from large variations in external pressure due to the absorption of all of the gas molecules [20]. However, a solution was proposed using virtual particles that experience only a strongly repulsive interaction with the polymer thereby behaving as a pressure regulating agent. Good agreement with experimental solubilities of oxygen were reported using this technique.

Recent work within the group is focusing on applying this technique using DL_POLY to the simulation of mixed gas diffusion. PET has been chosen as the polymer of interest because of its wide use in the packaging industry. However, diffusive processes through glassy polymers are

sufficiently slow as to render systematic simulation as function of several variables prohibitively expensive. As such, we begin by performing investigations in the melt regime well above T_g.

A parameterisation of PET was taken from the literature which displayed good agreement with experimental data for equation of state behaviour [21][22]. The most significant feature of this parameterisation is the use of the anisotropic united atom (AUA) model [23]. The AUA model differs from the simple isotropic united atom model by requiring that short range non-bonded interaction forces be calculated at a force site shifted a small distance away from the mass site. This adjustment essentially models the non-spherical geometry of many UA groups by modifying the non-bonded interactions to depend on the mutual orientation of the atoms involved as well as the separation distance. Such an adjustment necessarily generates a net torque about the centre of the parent atom. To resolve this, the total force on any atom involved in an interaction is balanced by complementary forces on its neighbouring atoms such that the net force across the group is equal to the original force as calculated at the geometric centre and the net torque is zero. The AUA model was originally applied to n-alkanes with a specific form of the force re-distribution equations which assumed that the two bonds joining any one carbon atom to its neighbours were both of equal length. To apply this model to PET, it was necessary to generalise this model such that an atom's bonds with its neighbours can be of different lengths. It was then necessary to modify DL_POLY to accommodate this new method of calculating van der Waals forces. An extra routine was created to be performed at the beginning of each timestep which would calculate the position of each atom's force site and extra geometry dependent terms required by the force re-distribution equations. In addition to a modification to existing routines for reading input files which processed the extra force site parameter without breaking backwards compatibility, the routine for calculating short range forces was modified to use the separation of geometric centres and perform the appropriate force re-distribution. Micro-canonical ensemble simulations of polyethylene and decane were performed to

check that the modifications did not introduce an energy drift either by producing a net torque or by generating forces inconsistent with the potential which produced them. The physical behaviour of the implementation was tested by replicating Toxvaerd's investigation into pressure scaling behaviour of n-alkanes.

< figure 4a and 4b side-by-side here>

Figure 4a illustrates the fact that the simple UA model is incapable of replicating this behaviour realistically. More accurate results may be obtained by re-parameterising the short-ranged interaction potential, as seen by the shift towards the experimental data of the second UA model (crosses) over the first (squares). However, the results deviate significantly at high volumes where the pressure is less well defined. This is resolved by the use of the AUA model which fits much more closely to the experimental data. This is most clearly shown by the use of a log-log scale in figure 4b. The UA datasets have equal gradients at low volumes but deviate away from linearity at the opposite end of the scale with the difference being a systematic pressure increase. In contrast, both the AUA sets of Toxvaerd (circles) and this work (pluses) have adjusted gradients to match the experimental line. It is also of note that this behaviour is ensemble independent having been tested in both NVT and NpT simulations. Besides enabling an accurate model of PET, there is interest in how the application of the AUA model affects the free volume distribution within the melt and, by extension, its effect on gas transport co-efficients.

The chosen parameterisation also required that DL_POLY be modified to accommodate a new torsional potential, $U(\varphi)$, and a different distance dependent dielectric function, $\varepsilon(r_{ij})$.

$$U(\phi) = \frac{1}{2}\sum_{i=1}^{2} A_i(1 + a_i \cos(b_i\phi)) \qquad (7)$$

Equation (7) is the revised torsional potential and requires the specification of six parameters for each dihedral angle. The parameters used are taken from quantum chemistry calculations by Boyd and Boyd [22].

$$\begin{aligned} \varepsilon(r_{ij}) &= 1 && r_{ij} < r_e \\ \varepsilon(r_{ij}) &= \varepsilon_B \exp\left[-\frac{r_e}{r_{ij}} \ln(\varepsilon_B) \right] && r_{ij} > r_e \end{aligned} \qquad (8)$$

Polarisation effects in PET are captured via a new distance dielectric constant (equation 8). DL_POLY is designed to be modular in nature allowing the user to easily modify or create only the routines relevant to the feature being implemented and then link them in with the rest of DL_POLY. As such, the extra dihedral potential and electrostatic potential necessitated the modification of only two subroutines. All modifications were tested by means of NVE energy conservation tests and backwards compatibility tests with existing DL_POLY simulation systems. The dihedral potential was also checked by verifying that the distribution of dihedral angles in a system employing the new potential was consistent with what was expected for that potential. Hedenqvist et al's simulated equation of state data for PET was then reproduced utilising the new code:

< figure 5 here >

The necessity of the application of the AUA model to PET is clearly shown by comparison to the equivalent UA points.

The final stage in the preparation of a basis for an investigation into the mixed gas effect was to verify that DL_POLY could perform the Kikuchi technique. Further modifications were required to implement the virtual particles in DL_POLY. These entailed a strongly repulsive non-bonded interaction parameterised by the z-axis separation of each virtual particle and any neighbouring polymer atoms. Constructing these systems for use within DL_POLY is then a multi-stage process. First, a polymer system must be constructed which is periodic in the *xy* plane only. Given the

difficulties associated with initialising a melt in standard three- dimensional boundary conditions, it was decided that an existing system would be manipulated to conform to slab boundary conditions. This entailed slowly extending the z-dimension length of the periodic box by one angstrom. Any larger increment would prevent the SHAKE algorithm from converging by making bonds which crossed the z-axis boundary unphysically large. Once a system has been reached in which no bonds cross the z-axis boundary, repulsive walls were applied to compress the system back to its equilibrium density. A cell of virtual atoms is then prepared with x and y dimensions which match the polymer system. The virtual atoms were assigned random positions with care taken to ensure that no atoms over- lapped with one another. This cell was then separately equilibrated in the NVT ensemble so that the virtual atoms had appropriate velocities. The interaction with the polymer is so strongly repulsive that an overly energetic system will quickly crush the melt. The two boxes were then spliced together with the virtual liquid cell positioned so that it wrapped around the box when the positions were minimum imaged thus sandwiching the polymer system. This new system was then equilibrated in the NpT ensemble so that the equilibrium virtual liquid phase volume could be determined. This volume was used in conjunction with the equation of state of the gas to determine the number of gas molecules which should be inserted into the virtual liquid phase to achieve the desired partial gas pressure. Since the gas molecules do not interact with the virtual liquid molecules, this process involved only copying and re-labelling existing virtual liquid molecules. It was found that these molecules need to be inserted such that their separation from the melt is greater than the non-bonded force cut-off distance otherwise the system breaks down as a result of the sudden increase in the system energy. The system then underwent a further period of equilibration to determine the evolution of the external pressure and whether any additional gas insertions were necessary before the production phase.

<figure 6 here>

Once the systems have been constructed, simulations performed using DL_POLY exhibit those features necessary to measure sorption processes. The first is the stability of the external partial gas pressure. Even at low concentrations, the simultaneous change in the volume of the virtual liquid phase and the number of gas molecules is sufficient to measure a well defined pressure based on the equation of state of the gas with fluctuations less than 1atm in magnitude. With this behaviour established, DL_POLY was used to verify Henry's Law for single gases as shown in figure 6. The relationship between the concentration of gas dissolved within the melt is shown to be linearly related to the average external gas pressure. Finally, a check on the numerical accuracy of the simulations was performed by comparing diffusion co-efficients measured at 600K to that reported by Pavel & Shanks [24] for NVT simulations at the same temperature. Values at each pressure were found to be comparable to those previously reported.

Acknowledgements

EPSRC is acknowledged for the funding of studentship funding for Dr. S Hotson, Dr. P Drew, and Mr. S. Butler whose PhD work forms the basis of the work in this manuscript. Funding through EPSRC GR/L37021 and EPSRC GR/L79229 is also acknowledged. Computer time accessed through the Leeds node of the White Rose University Consortium was used within this study.

References

[1] DL_POLY is a package of molecular simulation routines written by W. Smith and T. R. Forester, copyright CCLRC for the Central Laboratory of the Research Councils, Daresbury Laboratory at Daresbury, Nr. Warrington, 1996.
[2] K. Kostov, K. Freed, E.Webb, M. Mondello, G. Grest. *J. Chem. Phys.*, **108**, 9155 (1998).
[3] K. Karatasos, D. B. Adolf. *J. Chem. Phys.*, **112**, 8225 (2000).
[4] K. Karatasos, D. B. Adolf, S. Hotston. *J. Chem. Phys.*, **112**, 8695 (2000).
[5] S. Provencher, V. Dovi. *J. Biochem. Biophys. Methods*, **1**, 313 (1979).
[6] S. Provencher. *Comput. Phys. Commun.*, **27**, 213 (1982).
[7] H. Takeuchi, R. Roe. *J. Chem. Phys.*, 94, 7446 (1991).
[8] X. Qiu, M. Ediger. *Macromolecules*, **33,** 490 (2000).

[9] W. L. Jorgensen, J. Tirado-Rives. *J. Chem. Phys.*, **100**, 14508 (1996).
[10] M. G. Martin, J. I. Siepmann. *J. Chem. Phys.*, **102**, 2569 (1998).
[11] D. Steele. *J. Chem. Soc., Faraday Trans. 2*, **81**, 1077 (1985).
[12] J-P. Ryckaert, A. Bellemans. *Chem. Phys. Lett.,* **30**, 123 (1975).
[13] S. D. Hotston, D. B. Adolf, K. Karatasos. *J. Chem. Phys.*, **115**, 2359 (2001).
[14] P. M. Drew, D. B. Adolf. *Soft Matter*, **1**, 146 (2005).
[15] W. H. Stockmayer, W. Gobush, Y. Chikahisa, D. K. Carpenter. *Discuss. Faraday Soc.*, **49**, 182 (1970).
[16] A. V. Lyulin, G R. Davies, D. B. Adolf. *Macromolecules*, **33**, 3294 (2000).
[17] E. L. V. Lewis, R. A. Duckett, I. M. Ward, J. P. A. Fairclough, A. J. Ryan. *Polymer*, **44**, 1631 (2003).
[18] A. A. Gusev, U. W. Suter. *J. Chem. Phys.*, **99**, 2228 (1993).
[19] A. A. Gusev, S. Arizzi, U. W. Suter. *J. Chem. Phys.*, **99**, 2221 (1993).
[20] H. Kikuchi, S. Kuwajima, M. Fukada. *J. Chem. Phys.*, **115**, 6258 (2001).
[21] M. S. Hedenqvist, R. Bharadwaj, R. H. Boyd. *Macromolecules*, **31**, 1556 (1998).
[22] S. U. Boyd, R. H. Boyd. *Macromolecules*, **34**, 7219 (2001).
[23] S. Toxvaerd. *J. Chem. Phys.*, **93**, 4290 (1990).
[24] D. Pavel, R. Shanks. *Polymer*, **44**, 6713 (2003).

Captions

FIG. 1. DRTs at 400K for 50/20 systems at densities of (a) 0.29 gcm^{-3}, (b) 0.59 gcm^{-3}, and (c) 0.70 gcm^{-3}. c1 (○), c2, (△), c3(◇), c4(□), c5(▽), c6(⊕), c7(⊖), e-e vector (⌗). DRTs for intermediate vectors ck (20>k>7) are not shown for clarity. The estimated error on each point does not exceed the symbol size. Reproduced from *J. Chem. Phys*. **112**, 8225-8228, Copyright 2000, American Institute of Physics.

FIG. 2. DRTs at 400K for 10/100 systems at densities of (a) 0.29 gcm^{-3}, (b) 0.59 gcm^{-3}, and (c) 0.79 gcm^{-3}. $\mathbf{c}_1$ (○), $\mathbf{c}_2$, (△), $\mathbf{c}_3$(◇), $\mathbf{c}_4$(□), $\mathbf{c}_5$(▽), $\mathbf{c}_6$(⊕), $\mathbf{c}_7$(⊖), **e-e** vector (⌗). DRTs for intermediate vectors $\mathbf{c}_k$ (20>k>7) are not shown for clarity. The estimated error on each point does not exceed the symbol size. Reproduced from *J. Chem. Phys*. **112**, 8225-8228, Copyright 2000, American Institute of Physics.

FIG. 3. Intrinsic viscosity data for trifunctional dendrimers from the Green-Kubo viscosity formula (□), the direct intrinsic viscosity Green-Kubo formula (□), and the Brownian dynamics simulation results of Lyulin et al. (X). Data from Brownian dynamics correspond to the right hand axis and are in reduced units reported in the reference. Uncertainties are shown for the standard Green-Kubo analysis only, with all other errors being smaller than symbol size. Reproduced from Soft Matter 2005, 1, 146-151, 2005. by permission of The Royal Society of Chemistry

FIG 4a. NVT and NpT simulations of decane were performed at 673K to verify the accuracy of the AUA algorithm. Experimental data (dashed line), UA (□), UA with adjusted excluded volume parameters (×), AUA (+), AUA data of Toxvaerd (○). The estimated errors in the new data (□, ×, and +) are within the symbol size.

FIG 4b. Re-plotting the decane data with a log-log scale illustrates the exact effect and necessity of the AUA model. Symbols match figure 4a.

FIG 5. Equation of state behaviour for PET during NpT simulations at 597K. AUA (triangles), UA (squares), AUA Hedenqvist (circles)[20], experimental data (line)[20]. The estimated errors in the replicated data (triangles and squares) are within the symbol size.

FIG 6. Agreement with Henry's Law is shown for the relationship between the concentration of oxygen dissolved in PET and the external gas pressure at 600K.

FIG. 1

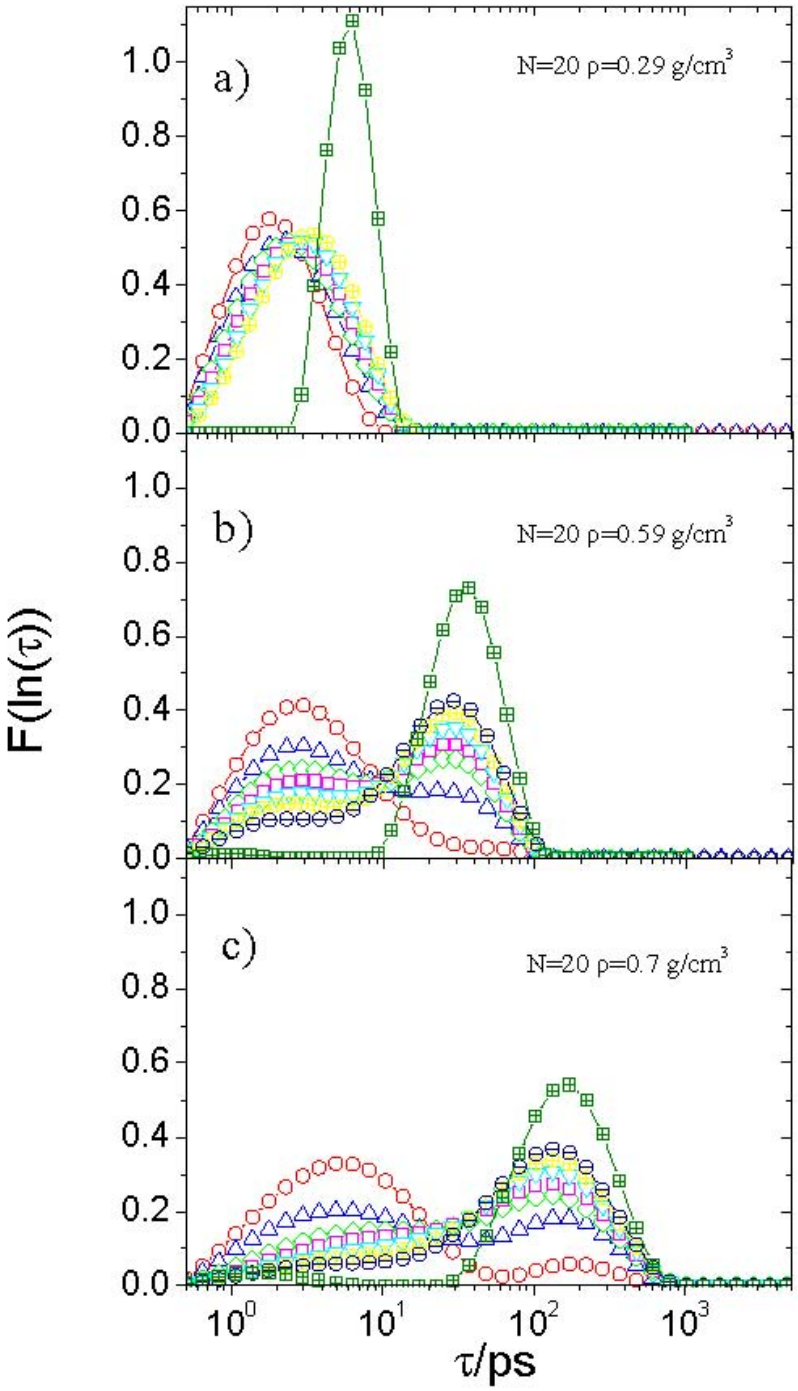
a)
N=20 ρ=0.29 g/cm^3
b)
N=20 ρ=0.59 g/cm^3
c)
N=20 ρ=0.7 g/cm^3
F(ln(τ))
τ/ps
1.0
0.8
0.6
0.4
0.2
0.0
10^0
10^1
10^2
10^3

FIG. 2.

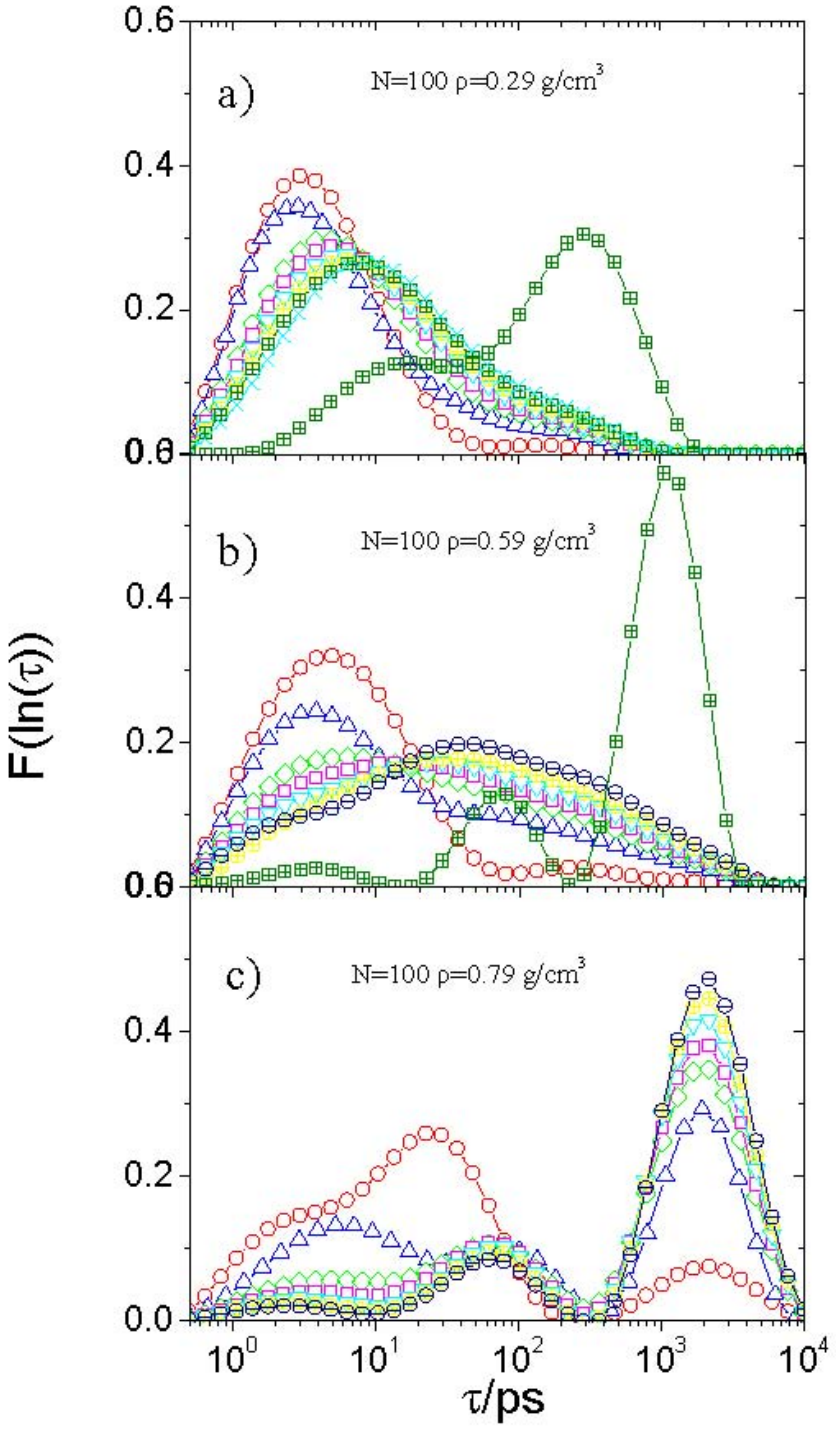
a)
N=100 ρ=0.29 g/cm3
b)
N=100 ρ=0.59 g/cm3
c)
N=100 ρ=0.79 g/cm3
F(ln(τ))
τ/ps
0.0
0.2
0.4
0.6
10^0
10^1
10^2
10^3
10^4

FIG. 3.

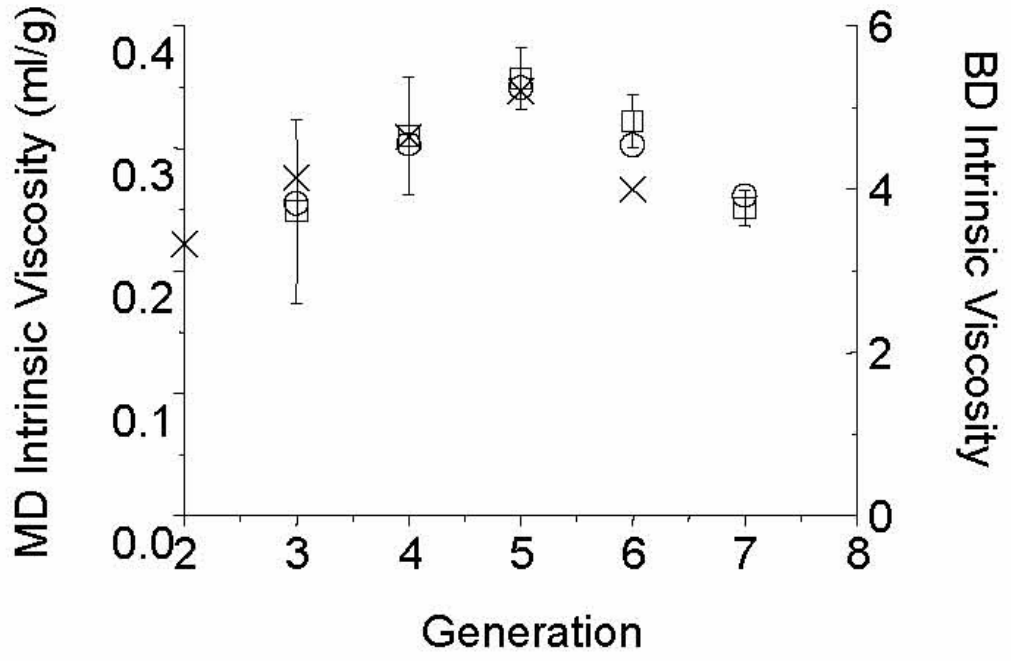
MD Intrinsic Viscosity (ml/g)
0.0
0.1
0.2
0.3
0.4
BD Intrinsic Viscosity
0
2
4
6
2
3
4
5
6
7
8
Generation

FIG 4a.

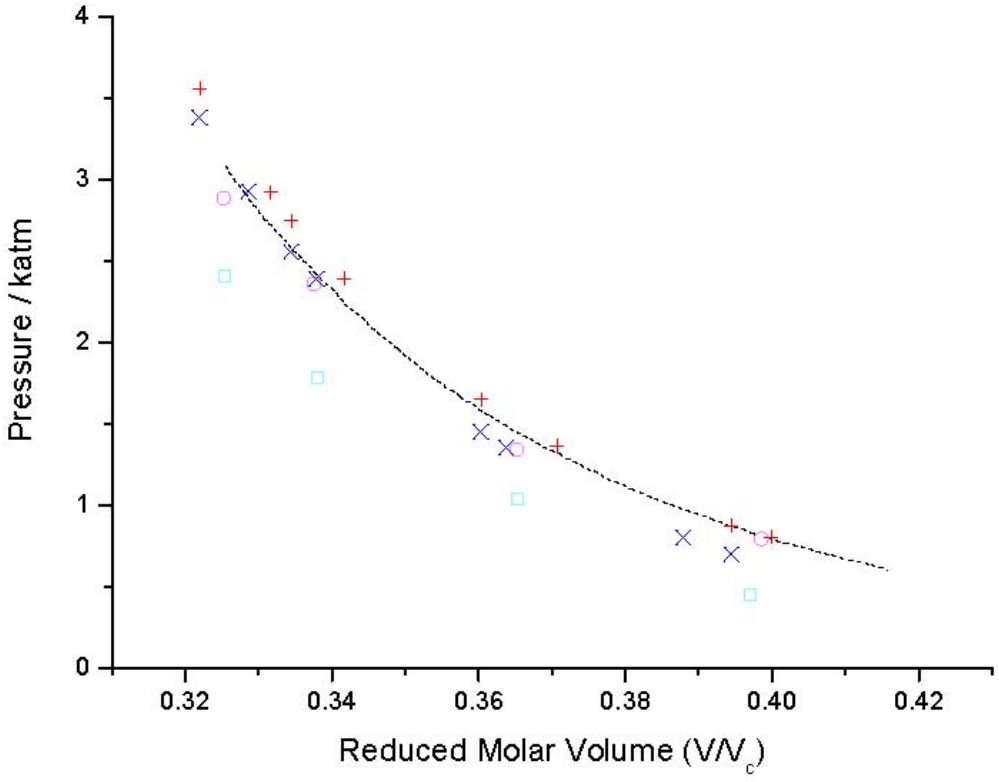
Pressure / katm
Reduced Molar Volume (V/V$_c$)
0
1
2
3
4
0.32
0.34
0.36
0.38
0.40
0.42

FIG 4b.

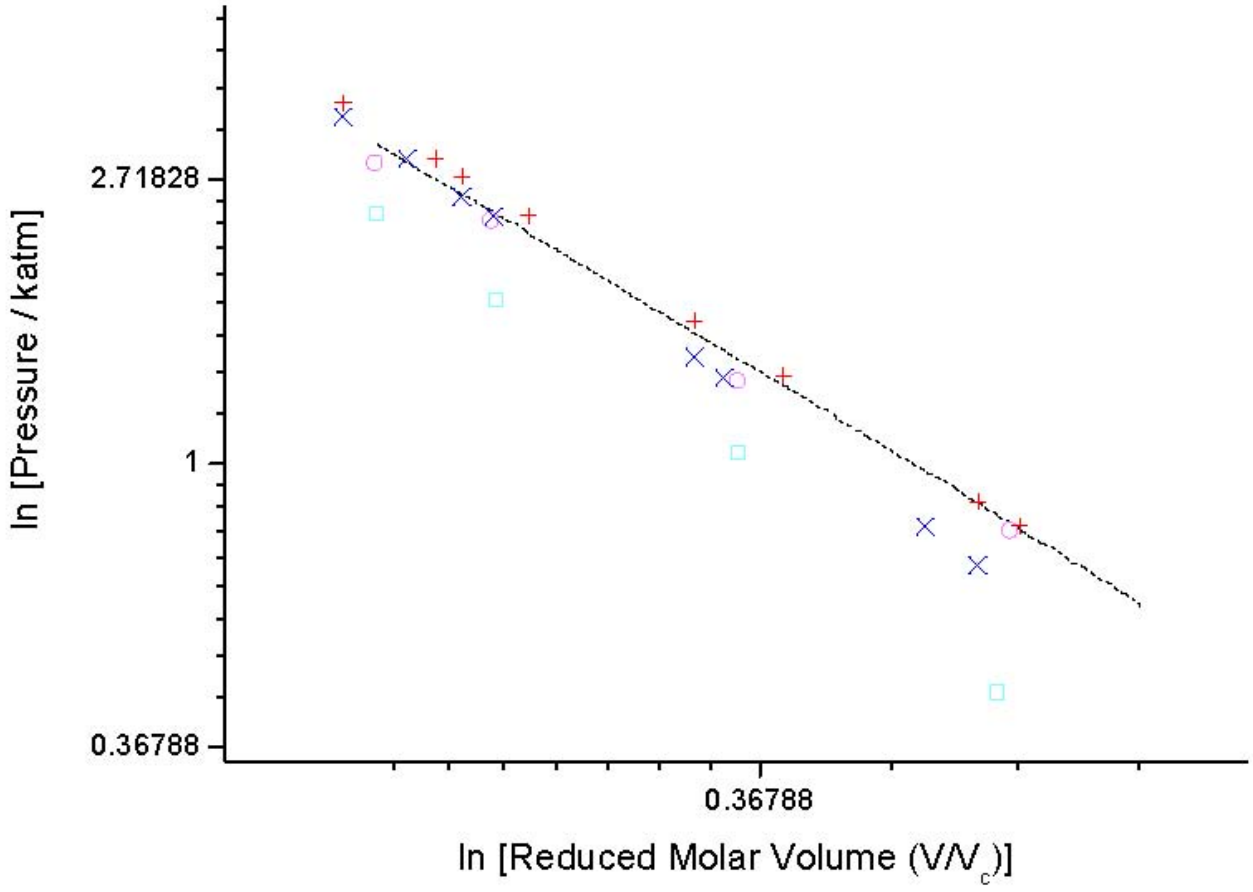
2.71828
1
0.36788
ln [Pressure / katm]
0.36788
ln [Reduced Molar Volume (V/V$_c$)]

FIG 5.

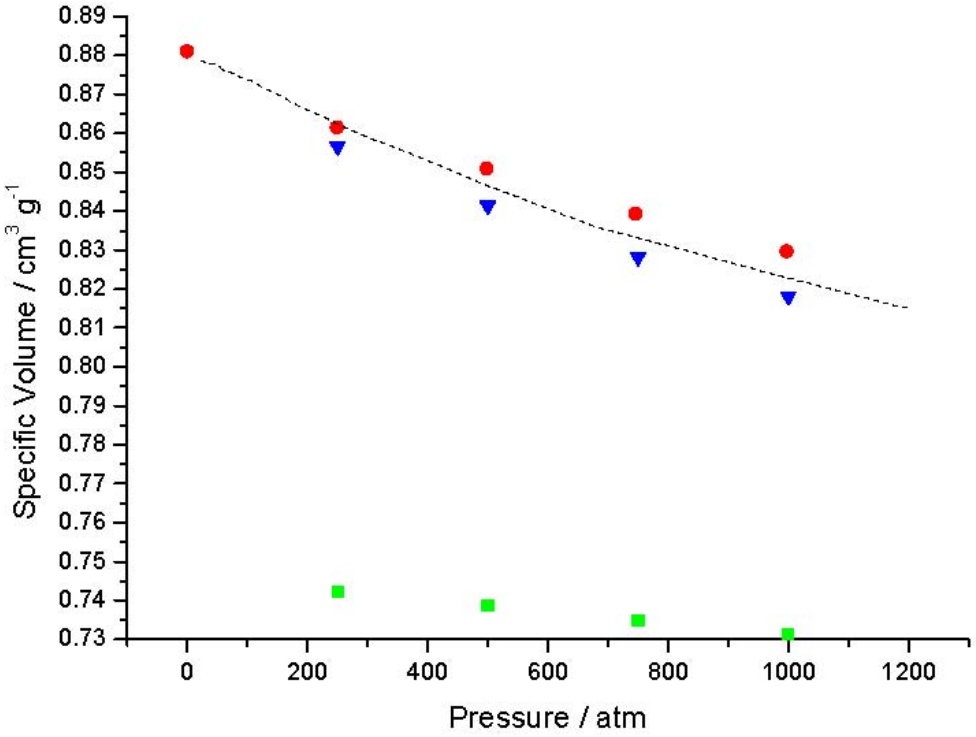
Specific Volume / cm^3 g^{-1}
0.89
0.88
0.87
0.86
0.85
0.84
0.83
0.82
0.81
0.80
0.79
0.78
0.77
0.76
0.75
0.74
0.73
0
200
400
600
800
1000
1200
Pressure / atm

FIG 6.

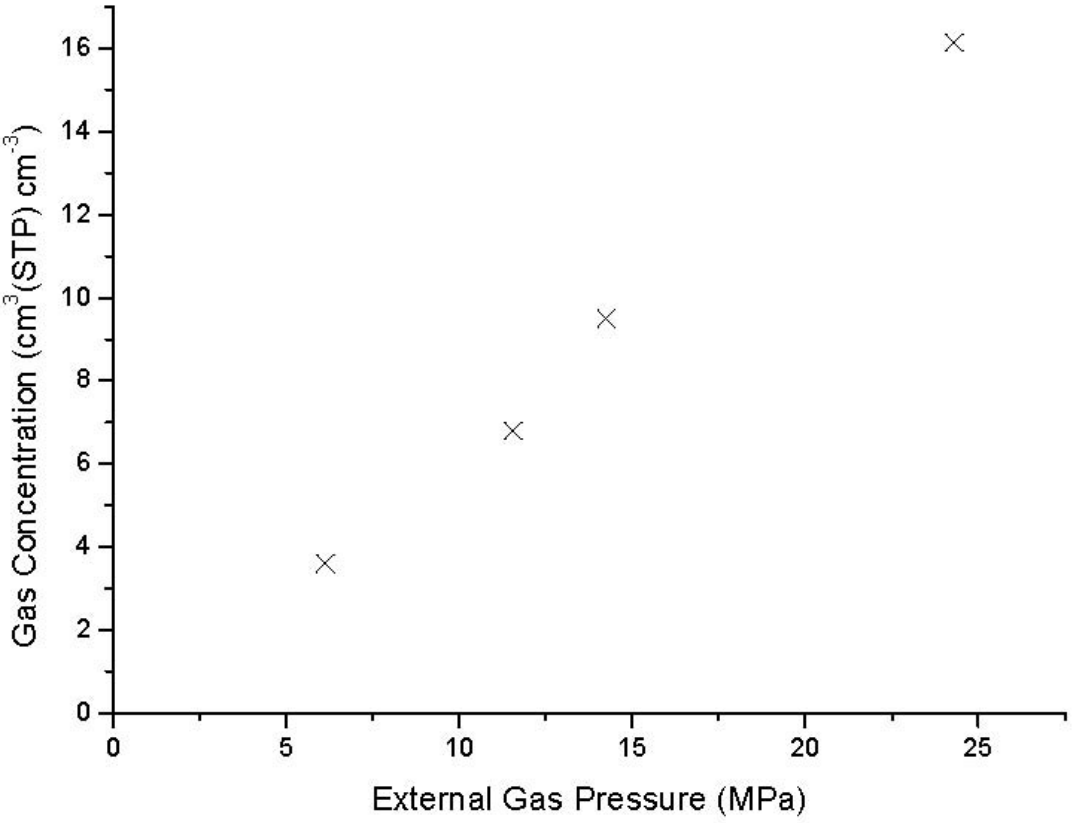
Gas Concentration (cm3(STP) cm-3)
External Gas Pressure (MPa)
0
2
4
6
8
10
12
14
16
0
5
10
15
20
25